Oxide Inclusions Formed in Steels (Report II)†
—Deoxidation Products by Nb, Zr, Cr, Complex Deoxidants—

Nobuya IWAMOTO*

Abstract

In the previous report (Trans. JWRI, 3 (1974), p. 41), the structural considerations of non-metallic inclusions formed when aluminium, silicon, manganese, titan and vanadium was added in molten steel were given. In this report, the problems when niobium, zirconium, chromium and complex deoxidants was added has been treated continuously.

1. Niobium

Niobium is a element which has become of major interest lately because it has effective behaviours to make austenite grains finely and the ability to prevent intergranular corrosion in austenitic stainless steels.

As for the nitrides of the system Nb-N, only two papers based on the reports of Brauer and his collaborators have been published: one by Brauer and Esselborn[109], another by Elliott[110]. Afterwards, Guard, Savage and Swarthout[111] have summarized this system in addition to these results. While, Brauer and Lesser[112), 113)] and Storms and Krikolian[114] have presented the results in regard to Nb-N system.

With respect to carbide, nitride and carbonitride formed in steels, Mori et al.[115] have been published.

As for oxides which has become a theme in this paper, there is a paper by Elliott[110]. Regarding to oxynitride there are two papers by Brauer[116]and by Brauer and Esselborn[109].

Besides, another reports concerning compounds included iron[112] and compounds included other metals[113] have been given.

There still remains the following undecided subjects until now:

1) Whether the oxide inclusion formed in steels containing low niobium is tapiolite ($FeTa_2O_6$) or columbite ($FeNb_2O_6$) of which the formation was reported by Mori et al.[115] or not?

2) Is it impossible to consider that NbO_2 are composed of mixture because there are some interplanar spacings which are difficult to index?

3) Niobium, titan, vanadium and chromium are elements which have ease of the reaction with nitrogen. It is said as for titan that there occurs separation of each phases of nitride and oxide not to take a structure of TiON. In opposition to this fact, the description of NbON is found in ASTM X-ray cards. From what reasons these differences are induced?

4) Whether there appears monoxide such as NbO[117] in steels containing high niobium content or not?

In **Table 7,** interplanar spacing values of oxide inclusions formed in steel containing 0.1 % niobium are compared with the result of tapiolite[118] and columbite[119), 120)]. It will be recogneized that there are no agreement between them.

Therefore, many sorts of mixtures having different FeO/Nb_2O_5 ratio have been heattreated in the atmosphere of argon at 1000°C. Their interplanar spacing values are given in **Table 8.** It will be anticipated that good agreement is noticed between specimen of $R=4$ and the values obtained from 0.1 % niobium containing steel. To certify the structural formula, it is hoped to study the valency state of niobium in these compounds.

In **Table 9,** the X-ray diffraction values of oxide inclusions extracted from 0.75 and 1 % niobium containing steels are compared with the results of NbO_2 whose values have been given by Brauer[116] and Elliott.[110]

In order to obtain the standard values of NbO_2, Nb_2O_5 as starting material was heattreated at various

Table 7. Interplanar spacing values of Inclusions extracted from 0.1 % ninbium containing steel.

Inclusions	Tapiolite	Columbite
2·970	3·35	3·74
2·882	2·58	3·61
2·596	2·37	3·41
2·515	2·27	2·92
2·383	2·12	2·81
2·211	1·75	2·55
2·085	1·678	2·50
1·897	1·546	2·45
1·774	1·503	2·42
1·751	1·411	2·32
1·722	1·405	2·26
1·687		2·20
1·533		2·17
1·467		2·05
1·452		1·98
		1·91
		1·87

† Received on July 3, 1974

* Professor

Table 8. Interplanar specing values of specimens heattreated at 1000°C in the atmosphere of argon. (R = FeO/Nb_2O_5 ratio)

Nb_2O_5 (β)		$R=1$		$R=3$		$R=4$		$R=5$		$R=9$	
d (Å)	I/I_0	d (Å)	I/I_0	d (Å)	I/I_0	d (Å)	I/I_0	d (Å)	I/I_0	d (Å)	I/I_0
3·177	8	2·966	100	2·966	100	2·970	100	2·999	11	3·033	11
2·834	22	2·871	13	2·864	11	2·871	14	2·969	30	2·797	100
2·783	32	2·797	12	2·797	56	2·799	37	2·761	101	2·615	72
2·713	11	2·531	21	2·609	42	2·615	24	2·609	71	2·590	31
2·542	12	2·496	15	2·554	* 14	2·542	44	2·560	24	2·485	27
2·496	6	2·377	9	2·525	16	2·496	16	2·289	16	2·372	9
2·313	20	2·318	* 4	2·490	17	2·381	7	2·120	8	2·294	24
2·074	12	2·230	4	2·377	* 10	2·292	* 5	2·105	8	2·149	48
2·059	17	2·208	9	2·285	* 9	2·233	* 4	1·908	36	2·105	* 11
2·044	17	2·078	9	2·230	* 5	2·221	8	1·755	44	1·912	42
1·915	40	2·059	4	2·208	11	2·155	2	1·732	* 8	1·757	42
1·789	* 7	1·915	8	2·078	10	2·109	* 10	1·719	8	1·712	* 10
1·776	5	1·896	7	1·905	17	2·080	8	1·651	11	1·665	* 10
1·742	6	1·831	* 6	1·896	11	1·909	* 11	1·631	11	1·658	16
1·700	12	1·794	6	1·831	* 8	1·897	* 9	1·540	36	1·651	* 15
1·686	28	1·776	15	1·773	17	1·831	7	1·507	26	1·542	39
1·581	20	1·732	18	1·752	* 11	1·796	4	1·499	8	1·518	32
1·558	7	1·722	24	1·732	21	1·778	15	1·464	4	1·509	34
1·531	5	1·686	* 8	1·719	25	1·754	14	1·451	6	1·469	* 11
1·453	* 5	1·673	* 6	1·538	17	1·732	* 18			1·306	9
1·406	8	1·616	4	1·529	16	1·722	25			1·389	10
1·397	* 10	1·581	* 5	1·506	* 15	1·623	* 7				
		1·529	14	1·481	6	1·540	* 8				
		1·483	* 6	1·461	14	1·530	15				
		1·463	9	1·451	24	1·509	* 9				
		1·379	5			1·491	* 11				
						1·464	11				
						1·452	19				
						1·380	4				

* diffuse pattern

Table 9. Interplanar spacing values of inclusions extracted from 0.75 and 1 % niobium containing steels.

0·75% Nb		1% Nb		NbO_2[121]		NbO_2[112]	
d (Å)	I/I_0	d (Å)	I/I_0	d (Å)	I/I_0	d (Å)	I/I_0
2·555	s	2·546	100	2·557	s	2·54	100
2·426	m	2·432	20	2·439	w	2·42	50
2·204	m	2·258	5	2·266	w	2·25	30
2·064	m	2·195	50	2·177	v v w	2·17	10
2·022	w	2·119	5	2·081	v w	1·76	100
1·757	s	1·759	80	1·762	s	1·71	70
1·714	w	1·713	30	1·717	s	1·62	20
1·552	w	1·553	40	1·551	v w	1·545	70
1·533	w	1·529	20	1·536	m	1·500	30
1·421	w	1·500	10	1·501	m	1·422	70
1·325	w	1·429	30	1·424	m	1·374	50
		1·375	10	1·374	m		
		1·324	40	1·319	v w		

time under the atmosphere of $H_2/N_2 = 5/1$. The variation of the interplanar spacing values are given in **Table 10.**

Furthermore, Nb_2O_5 was heattreated for 4 hours at the temperature of 750° and 800°C in the atmosphere of NH_3. Their interplanar spacing values are consistent with the results given by Brauer and Esselborn[109]. The results are given in **Table 11.**

To confirm the existence of NbO, the mixture of $Nb/Nb_2O_5 = 1/1$ was heattreated at 1500°C under the experimental conditions of 10^{-4}mmHg. The interplanar spacing values are given in **Table 12.**

Summarily, the oxide inclusion extracted from 10 % niobium containing steel was analysed from the results above described. The results are given in **Table 13.**

On the other hand, there exists undissolved problem concerning the formation of NbN having hexagonal structure. Brauer has studied it's behaviour in detail[122]. According to his paper, it is transformed to NbN having cubic structure above 1370°C by releasing nitrogen. However, heaxagonal structure is the stable form below 1370°C, and it has defect structure of $N/Nb < 1$. Accordingly, it has better to think that the appearance of hexagonal NbN is due to the precipitation from steel during solidification.

In **Fig. 9,** Nb(O·N) formed in steel was detected qualitatively by electron probe microanalyzer.

Table 10. Interplanar spacing values of Nb_2O_5 heattreated at 1300°C under the atmosphere of $H_2/N_2=5/1$ with various heating times.

30 min		2 hr		4 hr		6 hr		8 hr		12 hr	
d (Å)	I/I_0	d (Å)	I/I_0	d (Å)	I/I_0	d (Å)	I/I_0	d (Å)	I/I_0	d (Å)	NbN△
3·434	100	3·434	100	3·434	100	3·434	93	3·434	48	2·536	(111)
2·548	91	3·216	2	2·554	81	2·554	70	2·560	39	2·195	(200)
2·536	10	2·819	4	2·531	71	2·536	100△	2·542	100△	1·551	(220)
2·424	21	2·548	100	2·424	14	2·424	15	2·424	7	1·323	(311)
2·257	11	2·531	19	2·261	14	2·261	7	2·266	4		
2·191	6	2·424	27	2·191	39	2·195	86△	2·199	81△		
1·757	70	2·257	12	1·755	72	1·755	59	1·757	27		
1·712	23	2·195	12	1·712	23	1·712	15	1·710	5		
1·533	17	1·937	3	1·548	24	1·550	50△	1·552	48△		
1·529	11	1·899	2	1·531	14	1·529	7	1·527	5		
1·499	6	1·863	3	1·499	8			1·420	7		
1·421	17	1·797	3	1·421	12			1·377	4		
		1·755	81					1·323	39△		
		1·712	23								
		1·571	3								
		1·550	6								

△ NbN

Table 11. Interplanar spacing values of Nb_2O_5 heattreated at 750° and 800°C under the atmosphere of NH_3 for 4 hrs.

750°C		800°C	
(hkl)	d (Å)	d (Å)	I/I_0
111	2·496	2·496	100
200	2·156	2·160	98
220	1·527	1·526	44
311		1·294	26

Table 12. Interplanar spacing values of the specimen, $NbO_2/Nb=1/1$, heattreated at 1500°C under the experimental conditions of 10^{-4} mmHg.

NbO			NbO*[111]	
d (Å)	I/I_0	d (Å)	hkl	I/I_0
2·983	63	2·977	110	31·6
2·434	100	2·431	111	1·4
2·107	93	2·105	200	71·0
1·885	22	1·833	210	0·3
1·720	69	1·719	211	22·4
1·490		1·489	220	73·9

Table 13. Interplanar spacing values of inclusions extracted from 1 from 10 % niobium containing steel.

d (Å)	I	相			
2·893	w		hex-NbN		
2·579	w		hex-NbN		
2·425	s	NbO	hex-NbN	NbN	
2·225	s			NbN	
2·093	w	NbO	hex-NbN		
2·059	s				
2·023	m				Fe
1·967	m				
1·843	w		hex-NbN		
1·779	w				
1·472	w	NbO	hex-NbN		
1·391	w		hex-NbN		
1·352	m		hex-NbN		
1·310	m		hex-NbN		
1·255	m	NbO			
1·228	w				
1·203	m	NbO			

2. Zirconium

Zirconium is a stronger deoxidizer than aluminium. Furthermore, it's roll to remove sulphur and nitrogen from molten steel cannot be overlooked.

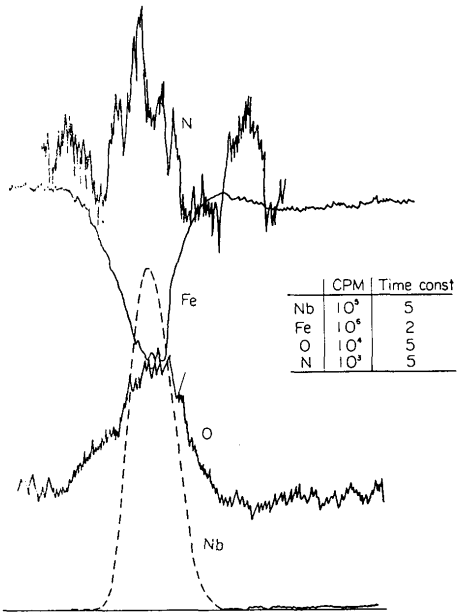

Fig. 9. XMA result of Nb(O·N) formed in steel.

Sims and Briggs[123] have informed the formation of zirconium silicate in addition to ZrO_2 when zirconium was added to molten steel. Then, they only say that stable ZrO_2 is formed at the time of deoxidation.

ZrO_2 itself transforms to tetragonal from monoclinic at about 1100°C. This transformation accompanying rapid volume change induces rupture of specimen. This is a troublesome problem when it is used as refractory, heating material and nuclear material. To prevent the transformation, it is usually forced to be cubic structure from adding another impurities based

on the experience[124)~129)]

It is unknown whether this sorts of thinking was given to analyse about the nature of ZrO_2 formed in steels. If stabilized ZrO_2 having cubic structure was formed in steels, one must consider the roll of impurities existed in steels to the deoxidation.

3. Chromium

When chromium is added to molten iron, it is important to know the behaviour ofchromium towards oxygen.

So far many investigations have been performed on the non-metallic inclusions formed in the alloys of Fe-Cr-O system. Among them, the study summarized by Hilty, Forgeng, and Folkman[130)] has been known widely, and the phase diagram of this system by Hansen[131)] is based on their results.

There exists another important problem concerning the possibility of chromium to be in a divalent state from the point of molecular crystal distortion, so-called Jahn-Teller effect.

The authors have been studying the formation mechanism of inclusions in Fe-Cr-O system from various viewpoints, and succeeded to complete a phase diagram of this system under the various oxygen partial pressures.

In this paper they summarized the results obtained hitherto as to the following items;

(1) Variation of primary inclusion by changing chromium contents in the alloy

(2) Behaviour of inclusions, subjected to various after-heat-treatments or solidifying velocities

(3) Establishment of the phase diagram of Fe-Cr-O system

(4) The Jahn-Teller effect on the tetragonal chromite by related studies to determine the variation of chromium valency

(5) Determination of the defect structure of chromite

All heats were made in high quality magnesia crucibles using a 15-kVA high frequency furnace at the pressure of 10^{-4} mmHg. Ferrochromium or electrolytic chromium was added to the melt aiming at the chromium contents of 0.7, 1.3, 2, 3, 5, 5.5, 6, 7, 8, 13, 18, and 65 %. All experiments were conducted mainly at a temperature of 1600°C.

The molten alloy was cast into water-cooled copper mould and the ingots of 15ϕ and 230 mm in length were obtained.

To obtain the phase diagram of Fe-Cr-O system, Fe_2O_3-Cr_2O_3 solid solutions made from the mixtures of desired ratios were reduced by CO_2-H_2 prepared in a gas mixer in the laboratory. The chemical compositions of starting materials are shown in **Table 14.**

In **Table 15,** the results of X-ray diffraction of the residues extracted from quenched specimens are given. From the lattice parameter reflected by (400) plane, it is found that the more increases the chromium content of residues, the greater becomes the lattice parameter a_0. The values calculated are given in **Table 16.**

Table 14. Composition of starting materials.

Starting materials	$(N_{Cr}/N_{Cr}+N_{Fe}) \times 100$
Ses 900	60.0
Ses 1 000	66.7
Ses 1 027	67.5
Ses 1 057	68.5
Ses 1 088	69.4
Ses 1 100	69.7
Ses 1 158	71.2
Ses 1 200	72.2
Ses 1 253	73.4
Ses 1 300	74.4

Tablet15. Interplanar spacings of isolated residues.

Nominal Cr (%)					
1.3	5	8	18	99.4	
	d(Å)				(hkl)
2.972	3.024	3.052	3.072	3.098	220
	2.942	2.927	2.914	2.873	202
2.531	2.565	2.583	2.601	2.611	311
	2.476	2.428	2.399	2.343	113
2.096	2.134	2.163	2.167	2.191	400
	2.017	1.986	1.936	1.897	004
1.711	1.729	1.733	1.738	1.744	422
1.613	1.613	1.609	1.607	1.600	333
	1.511	1.520	1.532	1.550	440
1.480	1.465	1.452	1.447	1.432	044

Table 16. Results of reflection from (400) planes.

Nominal Cr (%)	1.3	5	6	7	8	18	65	99.4
d(Å)	2.096	2.134	2.147	2.152	2.163	2.167	2.186	2.191
$a_{(400)}$	8.384	8.536	8.588	8.608	8.652	8.668	8.744	8.764

In **Fig. 10,** X-ray diffraction patterns of inclusions extracted from various sorts of chromium alloys are shown.

The lattice parameters a_0 and c_0 of the inclusions extracted from alloys of various chromium contents are shown in **Fig. 11.**

The distortion degree indicated by the c/a axial ratio changes from unity to 0.97 at 1.7 to 3 %Cr, 0.95 at 5 %Cr, 0.92 at 8 %Cr, and 0.89 at 13 to 18 %Cr and becomes 0.86 at 65 to 99.4 %.

The results summarized by Hilty, Forgeng, and Folkman[130], which are often referred as the most acceptable are as follows:

(1) (1) Low chromium, up to about 3 %Cr: $FeCr_2O_4$, which is a solid solution with Fe_3O_4 and $a_0=8.30$ Å.

(2) Medium chromium, 3 to 9 % Cr: distorted spinel and c/a=0.98 to 0.95, $a_0=8.39$ to 8.30 Å.

(3) High chromium: Cr_3O_4 and c/a=0.88 to 0.86, $a_0=8.64$ to 8.72 Å.

It is important that their distorted spinel is defferent from Cr_3O_4 and probably intermediate between $FeCr_2O_4$ and Cr_3O_4. Körber and Oelsen[132], Sims, Saller, and Boulger[133], and Linchevskij and Samarin[134] previously claimed an appearence of CrO in high chromium containing alloy.

Especially the present authors have paid attension to the existence of Cr_3O_4 or CrO at high temperature from a viewpoint of materials science, considering whether divalent chromium is stable or not.

In **Table 17,** the results of analysis on the effect of after-heat-treatments are given. In the case of 18 % chromium alloy, the change of the distortion degree from 0.89 to 0.92 was observed after the simple one hour treatment at 1000°C. This means a continuous change of the distortion degree of chromite.

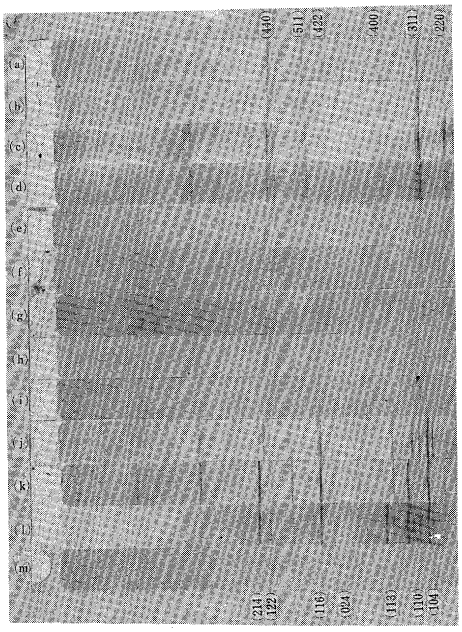

(a) Normal iron chromite
(b) Residue from 1.7 %Cr steel
(c) Residue from 3 %Cr steel
(d) Residure from below 5 %Cr steel
(e) Residue from 5 %Cr steel, treated at 1000°C×1 hr. and quenched
(f) Residue from 5.5 %Cr steel, alike treated
(g) Residue from 7 %Cr steel alike treated
(h) Residue from 8 %Cr steel alike treated
(i) Residue from 13 %Cr steel
(j) Residue from 18 %Cr steel
(k) Residue from 65 %Cr alloy
(l) Residue from molten chromium
(m) Chromic oxide

Fig. 10. X-ray diffraction patterns of the residue extracted from various chromium st els, 65 % chromium alloy and electrolytic chromium compared with normal iron chromite and chromic oxide (Cr K_α)

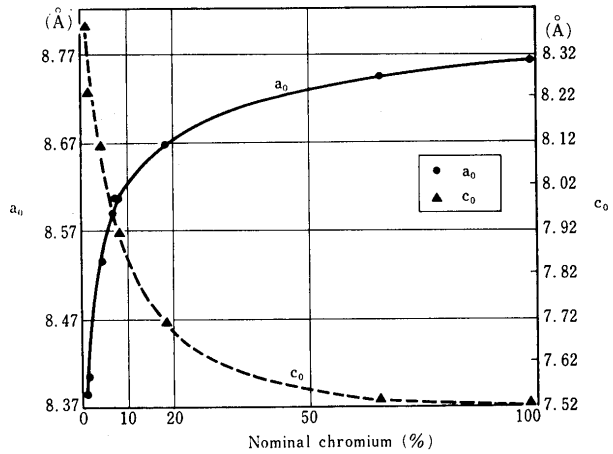

Fig. 11. The lattice parameters a_0 and c_0 of the inclusions extracted in comparison with chromium contents added to the specimens.

Table 17. Variation of inclusions with after-heattreatments.

Nominal Cr (%)	5	18
Primary	c/a=0.95 chromite	c/a=0.89 chromite
1 000°C×1 hr-Q.	c/a=0.95, Cr_2O_3	c/a=0.92, Cr_2O_3, $FeCr_2O_4$*
800°C×10 hr-F.C.	c/a=0.95 (20), Cr_2O_3, $FeCr_2O_4$	Cr_2O_3, $FeCr_2O_4$*
1 000°C×10 hr-F.C.	c/a=0.95 (20), Cr_2O_3, $FeCr_2O_4$	Cr_2O_3, $FeCr_2O_4$*
1 000°C×60 hr-F.C.	$FeCr_2O_4$, Cr_2O_3, c/a=0.95 (negl.)	Cr_2O_3, $FeCr_2O_4$*

Parenthesized value express relative intensities.
* Illustrates probably to contain c/a=0.97 iron chromite.

Table 18. Variation of inclusions with solidification velocities.

Nominal Cr (%)	5	18
Primary	c/a=0.95 chromite	c/a=0.89 chromite
Cast into graphite mould	c/a=0.95, Cr_2O_3 (10)	c/a=0.89 (30), c/a=0.95, Cr_2O_3 (30), $FeCr_2O_4$
Cast into sand mould	Reacted	Reacted
Crucible-solidified	c/a=0.95, Cr_2O_3 (40), $FeCr_2O_4$	c/a=0.95, Cr_2O_3 (80), $FeCr_2O_4$

Note: Parenthesized value express relative intensities.

In order to avoid the piling up of secondary precipitates in the case of after-heat-treatment of quanched specimen, and also the possibility of dissolving the precipitated α-Cr in the extraction process, if it exists as Hilty, et al. say[130], the extracted residues were heat-treated.

It was found that the primary inclusion from 18 % chromium decomposed to cubic chromite and chromic oxide whereas the inclusion from 65% chromium alloy only to chromic oxide. This suggests that an appearance of metallic chromium is difficult to be confirmed.

To know the influence of solidifying velocities on the structures of inclusions, the authors studied the variation of inclusions formed in alloys with solidification velocities. The results are shown in **Table 18.** Time-temperature curves of every specimen studied are shown in **Fig. 12.**

Figure 13 shows an example of the decaying of γ-ray for the inclusion extracted from 5 % chromium alloy and irradiated. It was impossible to compare the above with the profiles for chromium because the main peaks were induced by bromine contained in vinyl chloride used as a wrapper. The analysis of chromium could be made on the 65th day after the irradiation as shown in Fig. 12. Contents of Cr_2O_3 calculated from these results tabulated in **Table 19.**

The content of Cr_2O_3 in the inclusion extracted from 2 or 5 % chromium alloy is much smaller than that of the standard chromite ($FeCr_2O_4$, Cr_2O_3/FeO =67.7/32.3). Although it is liable to consider that the inclusions formed in the alloy of low chromium content

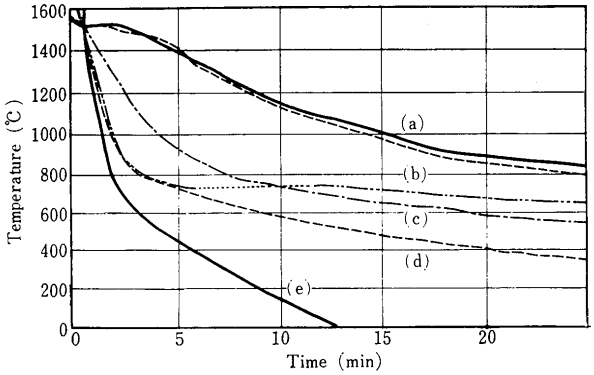

(a) Crucible-solidified
(b) Cast into iron mould with heater
(c) Cast into CO_2 process sand mould
(d) Cast into graphite mould
(e) Cast into water-cooled copper mould

Fig. 12. Solidification curves of various specimens.

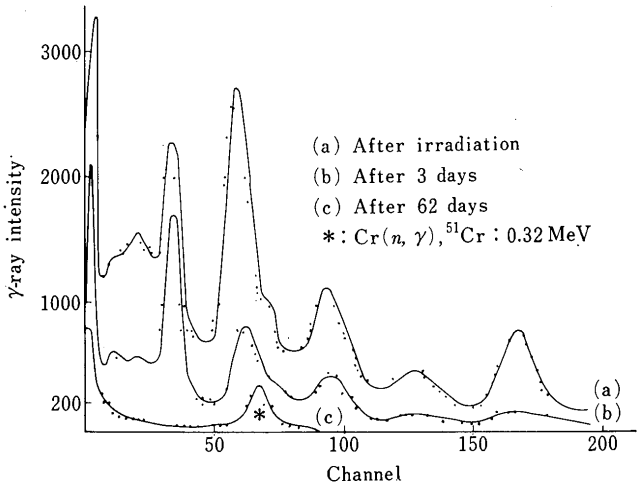

Fig. 13. Decaying γ-ray curve obtained by the use of inclusions extracted from 5 %Cr alloy and irradiated.

Table 19. Results of the activation analysis.

Sample	γ-ray abundance/ min. life time	Cr_2O_3 content (%)
Cr-1 mg	12 562±65	100
Cr-0.3 mg	3 819±42	100
$FeCr_2O_4$	5 525±52	67.7
*F**-8**-1***	7 867±74	93.4
*P**-18-1	6 865±65	83.2
P - 5-1	6 436±58	77.4
F -18-1	6 134±56	74.5
F - 5-5	3 533±79	47.5
F - 5-4	4 870±57	59.9
F - 5-3	4 733±60	56.9
F - 5-1	2 836±38	38.0
F - 2-1	3 071±54	40.2
F -18-3	2 883±50	39.4
F -18-4	1 763±37	25.6

* *F* and *P* represent the types of chromium added, ferro-chromium and electrolytic chromium

** 8, 18, 5, and 2 represent chromium content in the alloys

*** 1, 3, 4, and 5 represent quenched, heat-treated at 1000°C for 10 hr, 800°C for 10 hr, and 1000°C for 60 hr.

are composed of a solid solution of iron chromite and magnetite, such a presumption is not accepted from the results of the lattice parameter measurement of the inclusions and from the fact that the tetragonal chromite decomposes to iron chromite and $(Fe\cdot Cr)_2O_3$ by the subsequent heat treatments. It must be mentioned here why the Cr_2O_3 content in the inclusion in 8 % chromium alloy is extraordinarily high as 93 %. This is consistent with the fact that the solubility of oxygen in molten iron-chromium alloy reaches a minimum at the composition near 8 % chromium. It may be regarded that the valence states of elements contained in the inclusions are determined by the partial pressure of oxygen equilibrated with molten iron-chromium alloy. The content of Cr_2O_3 in inclusions formed in high chromium alloys are much higher than that of the standard chromite. It seems to be consistent with the presumption that iron in the inclusions can be substituted by chromium. However, it will be an important problem in the field of solid state physics, if there is a possibility that chromium has a divalent state.

The next obvious result is that the content of Cr_2O_3 in the inclusion extracted from after-heat-treated low chromium alloy, is higher than that of the sample as quenched, in contrast to the high chromium alloy. From the experimental evidence confirmed by X-ray analysis, one can accept an appearance of Cr_2O_3 as the secondary precipitate for the case of high chromium alloy, that is, the total Cr_2O_3 content in the inclusion formed must be higher by the after-heat-treatment. Since the actual total content of Cr_2O_3 decreases by contraries, there seems to be an exchange of the elements between the matrix and inclusions during the heat treatment process.

Likewise, in the case of low chromium alloy, it is not able to interpret the content of Cr_2O_3 in the inclusion extracted from after-heat-treated alloys is higher than that of stoichiometric $FeCr_2O_4$ even if it is mainly the secondary precipitate of $FeCr_2O_4$.

However, the result that the content of Cr_2O_3 in the inclusion formed in the as-quenched high chromium alloy is higher than that of stoichiometric $FeCr_2O_4$ is consistent with that of the composition of synthetic chromite.

To clarify the formation mechanism of tetragonal chromite in iron-chromium alloys, the reduction of $(Fe\cdot Cr)_2O_3$ solid solutions were tried by the use of H_2-CO_2 mixed gas at 1600° to 1850°C. The dependency of the tetragonality of chromite on oxygen partial pressure, chromium content of chromite and reducing temperature was obtained.

In **Fig. 14,** the relationship between the composition of starting materials and oxygen partial pressure at 1600°C is given. It is seen that tetragonal chromite is a typical nonstoichiometric compound.

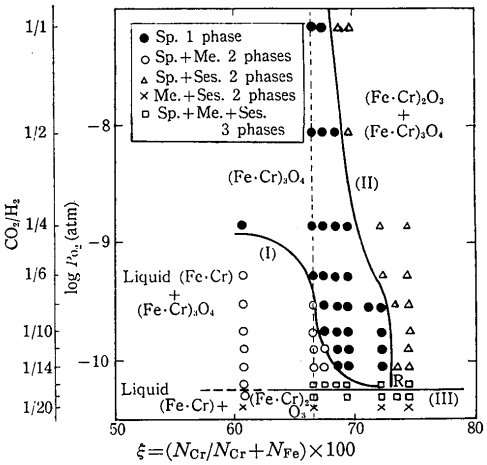

Fig. 14. Log $Po_2-\xi$ phase diagram at 1600°C.

In **Fig. 15,** the influence of gas mixing ratio and the composition of starting material on the lattice parameter a_0 is shown. It is found that the tetragonality of chromite becomes smaller with decrease of the oxygen partial pressure and with increase of chromium content of chromite.

With the rise of the treating temperature up to 1700°C, the single phase region of tetragonal chromite with axial ratio smaller than 0.95 was formed.

Furthermore, the reduction experiments at higher temperature of 1800°C were performed. The X-ray diffraction result of the reduced product by hydrogen at 1850°C are given in **Table 20.**

The relationship between lattice parameters, a_0 and c_0, and the tetragonality is expressed by the following equations:

$$a=\frac{a_0}{\gamma}\left(\frac{1+2\gamma^2}{3}\right)^{1/2} \quad (1)$$

$$c=a_0\left(\frac{1+2\gamma^2}{3}\right)^{1/2} \quad (2)$$

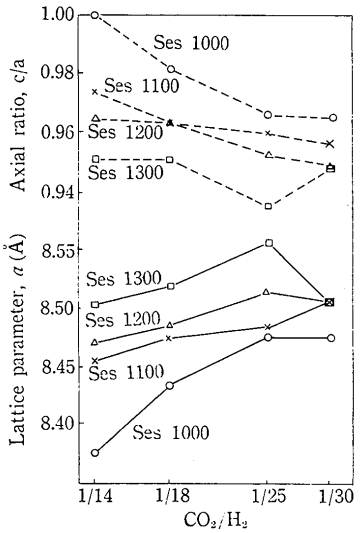

Fig. 15. Dependence of axial ratio and lattice parameter of chromite on the gas mixing ratio.

Table 20. X-ray analysis results of Ses 1000 reduced in H_2 at 1850°C.

d(Å)	Tetragonal Chromite (hkl)	Cr_2O_3 d(Å)	Cr_2O_3 (hkl)	Inclusion from 18% Cr alloy
3.096	220			3.072
2.908	022			2.909
2.670		2.666	014	2.671
2.589	311			2.596
2.487		2.480	110	2.484
2.399	113			2.399
2.172	400	2.175	113	2.172
2.034				
1.813		1.816	204	1.818
1.737	422			1.738
1.673		1.673	116	1.674
1.659	511			1.663
1.606	333			1.604
1.532	440			1.533
1.464		1.465	124	1.466
1.450	044			1.447
1.437		1.432	300	

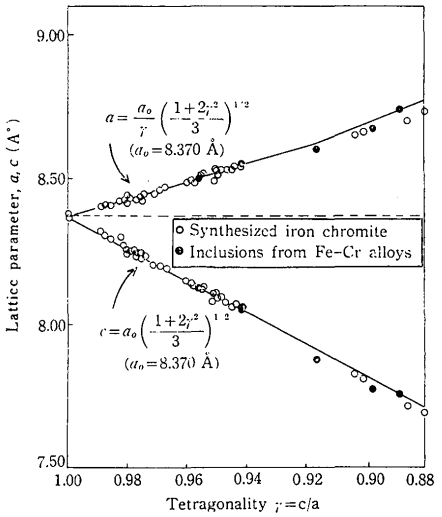

Fig. 16. Relationship between of lattice parameters and tetragonality.

where γ is tetragonality and a_0 is 8.37 Å of cubic chromite. In **Fig. 16,** the dependence of lattice parameters, a and c, on tetragonality $\gamma = c/a$ is shown. However, a slight deviation from the relation was found with an increase of tetragonality.

Hilty et al. have reported[130] the stability of Cr_3O_4 above 1600°C. To clarify the formation of this oxide, the author, Takano and Adachi[155] studied the reduction product of Cr_2O_3 at 1600° to 1850°C.

It is expected to obtain Cr_3O_4 from the mixture composed of the constant ratio of chromium and Cr_2O_3 in an inert gas or vacuum or as the reduction product from Cr_2O_3 if it is a stable phase above 1600°C. The purity of inert gas used is important, as the equilibrating oxygen partial pressure is exceedingly low and, furthermore, the effect of the solidifying velocity of specimen should be considered if there exists the possibility of Cr_3O_4 to decompose to metallic chromium and Cr_2O_3 near 1600°C.

The reduction products of Cr_2O_3 and $(Fe \cdot Cr)_2O_3$ solid solution by graphite in an atmosphere of nitrogen or argon are shown in **Table 21.** Cr_3O_4 was impossible to be detected in the reduction product of Cr_2O_3 at 1600° to 1850°C. This result agrees with that by Muan[135].

When a transition metal ion is surrounded by negative ions, the five d orbitals no longer have the same energy but are split into two groups, a triplet t_{2g} and a doublet e_g[136]. This is shown in **Fig. 17.** The physical basis for this splitting is simply an electrostatic repulsion between d-electrons and surrounding negative ions. Jahn and Teller[137] showed that the structure became unstable and distorted, providing a sufficient asymmetry to lift the degeneracy, if there was a degenerate orbital state associated with the localized d-electrons at a transition-metal cation in a polar crystal. The distortions in the octahedrons and the tetrahedrons result from this effect.

Dunitz and Orgel[138] summarized the stabilization in the crystal field energy for each configuration of d-electrons as shown in **Table 22.**

From this table, certain qualitative conclusions can be drawn for the relative stability of transition-metal ions in these sites. Large distortions from the regular tetrahedral symmetry are expected to occur only for the configurations, $(e)^2(t_2)$, $(e)^2(t_2)^2$, $(e)^4(t_2)^4$, and $(e)^4(t_2)^5$ produced by 3, 4, 8, and 9 d-electrons, respectively.

Although the structure is not known yet, Dunitz and Orgel suggested the existence of CrO which showed a slight departure from the cubic symmetry at sufficiently high temperatures and probably has the structure of CuO type. In addition, they showed that the distortion might occur in the tetragonal arrangement for the case of Cr^{2+}.

There are several methods for determining the cationic arrangement of the crystal site, such as the precision measurement of the lattice parameter, the measurement of the X-ray intensity and infrared adsorption, *etc.*

In order to determine an accurate X-ray intensity, it is necessary to utilize an abnormal dispersion. However, this was not applied yet because the difference between chromium and iron is not sufficient.

Oonishi and Teranishi[139] found that the unit cell volume was kept nearly constant in the cubic as well as in the tetragonal regions which are due to the Jahn-Teller effect between $CuFe_2O_4$ and $CuCr_2O_4$. Furthermore, they showed that the lattice parameter changed drastically at the transition point of the crystal structure. In connection with this, the authors also

Table 21. X-ray results of the reduction products by graphite.

Starting materials	Mixed ratio of graphite	Atmosphere	Result
Cr_2O_3	1.0C	Ar	Cr_2O_3, Cr
$0.98Cr_2O_3-0.02Fe_2O_3$	1.0C	N_2	Cr_2O_3, Cr_2N
$0.98Cr_2O_3-0.02Fe_2O_3$	3.0C	N_2	Cr_2N, Cr
$0.90Cr_2O_3-0.10Fe_2O_3$	1.0C	N_2	Cr_2O_3, (FeCr)
$0.74Cr_2O_3-0.26Fe_2O_3$	1.0C	N_2	Cr_2O_3, (FeCr)
Ses 1 100	0.3C	Ar	Chromite (c/a=1~0.98)

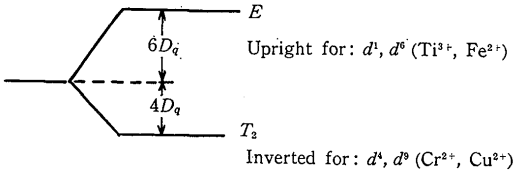

Fig. 17. Splitting diagrams for *d* orbitals.

Table 22. Configuration of Jahn-Teller distortion.[10]

Number of *d*-electrons	Octahedral		Tetrahedral	
	Configuration	Distortion	Configuration	Distortion
1	(t_{2g})	*a*	(e)	*a*
2	$(t_{2g})^2$	*a*	$(e)^2$	*o*
3	$(t_{2g})^3$	*o*	$(e)^2(t_2)$	*b*
4	$(t_{2g})^3(e_g)$	*b*	$(e)^2(t_2)^2$	*c*
5	$(t_{2g})^3(e_g)^2$	*o*	$(e)^2(t_2)^3$	*o*
6	$(t_{2g})^4(e_g)^2$	*a*	$(e)^3(t_2)^3$	*a*
7	$(t_{2g})^5(e_g)^2$	*a*	$(e)^4(t_2)^3$	*o*
8	$(t_{2g})^6(e_g)^2$	*o*	$(e)^4(t_2)^4$	*b*
9	$(t_{2g})^6(e_g)^3$	*b*	$(e)^4(t_2)^5$	*c*

o: zero distortion, *a*: small distortion
b: large distortion c/a>1
c: large distortion c/a<1

found that there was an abrupt change in the lattice parameter of the tetragonal chromite when the lattice parameter was plotted against $(N_{Cr}/N_{Cr}+N_{Fe})$, which is shown in **Fig. 18.** This will indicate that the Jahn-Teller effect contributes to the tetragonal chromite.

Mn_3O_4 and $ZnMn_2O_4$ are only examples with high Jahn-Teller transition temperatures such as 1075° to 1157°C or 950° to 1125°C[140]. To determine whether the effect gives a contribution to the tetragonal chromite or not, the high temperature X-ray diffraction study has been made on the inclusions with the axial ratios, *c/a*, of 0.95 and 0.89 which were extracted from 5 and 18% chromium alloys. It was found that the tetragonal chromite decomposed to cubic chromite and $(Fe\cdot Cr)_2O_3$ at temperatures higher than 700°C. Although this result seems to disagree with the findings in Fig. 9, it is necessary to consider the effect of oxygen contained under the experimental conditions of X-ray diffraction. It is intended to carry out the

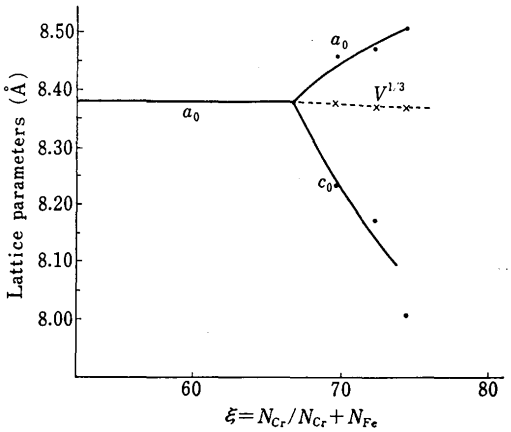

Fig. 18. Variation of lattice parameter with ξ.

study at lower temperatures precisely.

The valence state of iron contained in chromite must be changed from Fe^{3+} to Fe^{2+} in order to take a tetragonal structure. To confirm the transferability of Fe^{3+} to Fe^{2+} in chromite, the Mössabuer resonanse has been measured in the current work.

The Mössbauer resonance study gives an information about the strength and the angular distribution of binding, the magnetic and electronic fields and the density of *s*-electrons around a nucleus[141]. Isomer shift caused by the difference of nuclear radii of the ground and excited states show a change in the density of *s*-electron resulted from the change in valence, which is accompanied with the change in the coulombic interaction appearing as a shift of the nuclear levels. The relation is shown in **Fig. 19.**

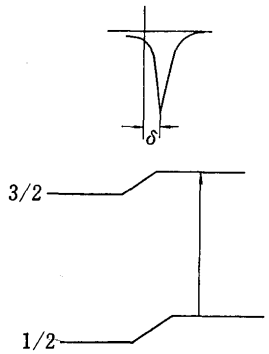

Fig. 19. Isomer shift.

Furthermore, all or a part of the $2I+1$ fold degeneracy (I: nuclear-spin quatum number) is lifted in case that the nucleus is not spherical and the density of the charged electrons is not uniform. The non-vanishing term induced by the electrostatic interaction between the nucleus and the surrounding charged electrons is a cause of the quadrupole splitting. This is caused by the nuclear quadrupole moment, reflecting the deviation from the spherical symmetry of nucleus. The quadrupole splitting is schematically represented in **Fig. 20.**

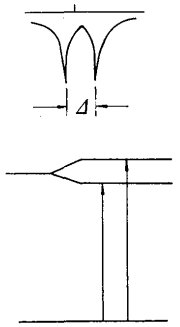

Fig. 20. Quadrupole splitting.

Chromite with the axial ratios ranging from unity to 0.90 and the inclusions extracted from chromium alloys were subjected to the measurement of Mössbauer resonance. The representative resonance peaks are shown in **Fig. 21** as compared with the previously determined values. The values of quadrupole splitting are also given in **Table 22.**

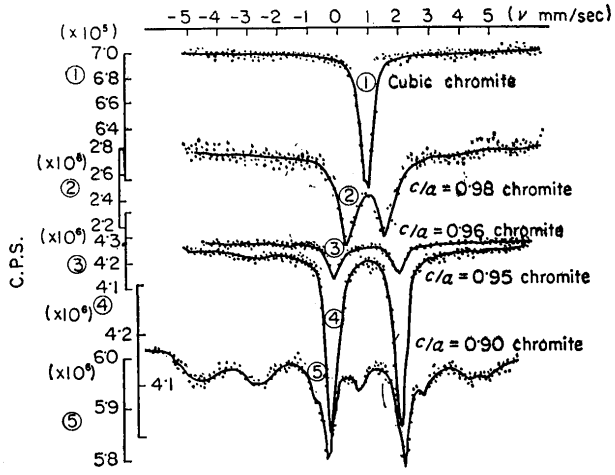

Fig. 21. Mössbauer spectra.

Table 23. Mössbauer parameters.

Sample	Isomer shift (d mm/sec)	Peak separation (Δ mm/sec)
$FeCr_2O_4$	0.957	0.0
c/a=0.98*	0.913	1.25
c/a=0.96*	0.892	2.04
c/a=0.95*	0.913	2.25
c/a=0.90*	0.913	2.37

* Illustrates tetragonal chromite

To clarify the defect structure of tetragonal chromite, it is necessary to use the thermogravimetry of the reduction process from $(Fe\cdot Cr)_2O_3$ solid solution or the oxidation process from tetragonal chromite, the density measurement and chemical analysis.

As an example, the reduction curves of $(Fe\cdot Cr)_2O_3$ solid solution with $\xi=0.667$ under a stream of H_2-CO_2 gaseous mixture are shown in **Fig. 22.** It is seen that the equilibrating conditions are attained within 5 to 15 min.

In **Table 24,** the weight gain by oxidation is compared with the calculated one.

From this measurement, it seems apposite to consider that the cubic and tetragonal chromite have defect structures. This is consistent with the result obtained from the density measurement that the composition of tetragonal chromite with 0.95 axial ratio is $(Fe_{0.26}\cdot Cr_{0.74})_{3.04}O_4$.

Furthermore, Iwamoto, Takano, and Adachi have studied the electrical resistivity and thermo-electromotive force under the various reducing conditions to confirm a defect structure of tetragonal chromite. The result is shown in **Fig. 23.**

Compared with the result of phase diagram, it is seen that the oxygen defect increases with decrease of

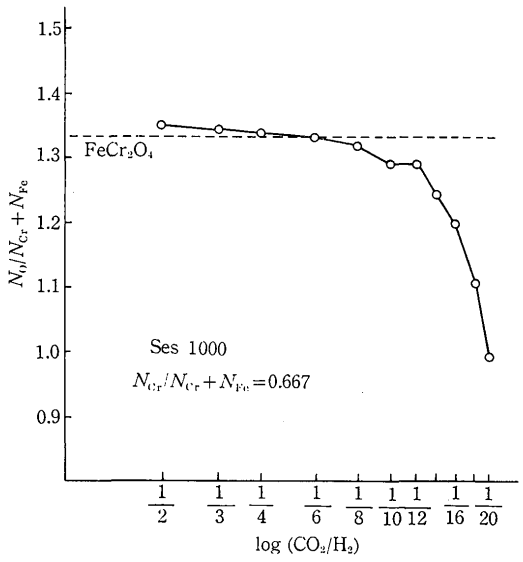

Fig. 22. Reduction curves of $(Fe\cdot Cr)_2O_3$ solid solution in CO_2-H_2 mixing gas.

Table 24. Oxidation study result (1070°C, 10°C/min).

Sample	Initial weight (mg)	Weight gain (mg)	Calculated
$FeCr_2O_4$	114.9	5.8	4.08
$Fe+Cr_2O_3$	128.7	14.0	14.0
c/a=0.97*	52.4	3.9	
c/a=0.95*	108.0	8.3	

* Illustrates tatragonal chromite

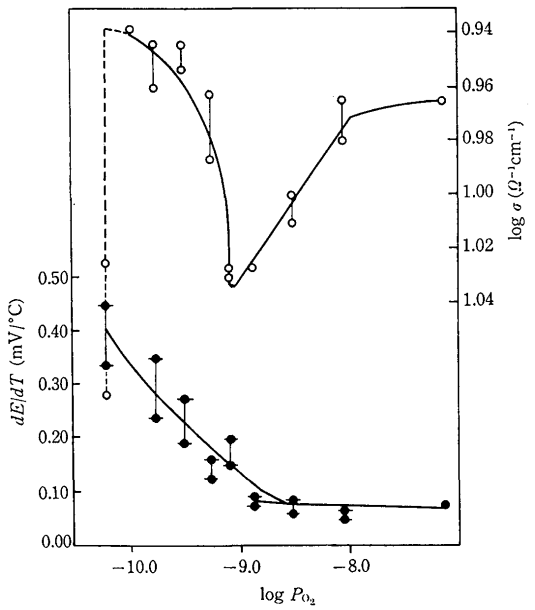

Fig. 23. Log σ and dE/dT-log P_{O_2}.

oxygen partial pressure in spite of a single phase of cubic chromite. The electrical conductivity of tetragonal chromite was found to be proportional to $-1/2(n+1)$ power of the oxygen partial pressure when the thermodynamic equilibrium was attained. The disorder in cubic chromite may be described as follows:

$$\sigma = K_1 P_{O_2}^{-1/2(n+1)}$$

In the tetragonal region, the defect type changes to P-type conductor and the thermoelectromotive force also shows the same tendency. It must be emphasized that more study is necessary to clarify the formation mechanism of tetragonal chromite.

It is well known that the study on the X-ray peak shift is effective to determine a change in the valence of an element. Tanaka and Okuno[142] measured the values of K emission wave-lengths of the compounds containing iron. However, the variation of the shift observed was just small, regardless of the variation of the valence. On the study of the compounds of chromium, they found that there is a significant shift on the contrary to iron compounds[143]. Meisel and Nefedow[144], Menshikov[145], and Meisel and Trong[146] investigated in detail on this matter. Among them, Meisel and Trong summarized the results as follows:

(1) Width of K_α doublet for Cr^{3+} is larger than that for Cr^{2+}.

(2) K_α line of the compounds containing Cr^{2+} shifts to a shorter wave-length as compared with the Cr^{3+} shift.

The results of K_α doublet shift and half-width for the synthesized tetragonal chromite are shown in **Table 25.** It was found that there is no significant difference in the iron K_α shift corresponding to the variation of the tetragonality of chromite. Although an attempt has been made to separate the $CrK_{\alpha 1}$ and $CrK_{\alpha 2}$ profiles, it was too dull to determine $K_{\alpha 2}$ shift. The measurement of the K_α doublet shift shows that the CrK_α doublet shift of Cr_2O_3, and cubic and tetragonal chromites appeared in the longer wave-length as compared with that of standard metallic chromium, and that the amount of shift was proportional to the tetragonality of chromite. If the $K_{\alpha 2}$-$K_{\alpha 1}$ is defined to be the quantity of K_α doublet shift, the existence of Cr^{2+} in the tetragonal chromite may be explained from the behaviour of peak shift observed in comparison with those reported by Meisel and Trong (although there are some questions on that an ionic crystal is used as the standard sample for Cr^{2+} determination).

According to the crystal field theory, D_q for various transition-metal ions and coordination types can be calculated. In **Table 26,** their values are given[147].

The near infrared absorption results obtained for Cr_2O_3, cubic and tetragonal chromite are shown in **Fig. 24.** Cr_2O_3 showed an absorption band at 8700 cm^{-1} as well as cubic chromite. However, the tetragonal chromite showed a shift of the absorption band such as 8000 to 8330 cm^{-1}. From these results, it was impossible to conclude what sort of ions can occupy the tetrahedral position. It is necessary to consider the influence of the redistribution of electron density in

Table 25. Asymmetry index, half-width and peak shift of CrK_α doublet.

Specimen	α_5	H_W (mm)	(deg)	P_S (deg)
c/a=0.90	1.14	27.5	0.6875	−0.05
c/a=0.95	1.14	27.5	0.6875	−0.05
c/a=0.96	1.09	27.5	0.6875	−0.04
c/a=0.98	1.06	27.5	0.6875	−0.03
c/a=0.98	1.08	27.5	0.6875	−0.03
$FeCr_2O_4$	1.05	27.3	0.6825	−0.03
Cr_2O_3	1.05	26.3	0.6575	−0.01
$(Fe\cdot Cr)_2O_3$	1.04	26.0	0.6500	−0.01
Cr	1.01	25.6	0.6400	0.00

Tabm Table 26. Crystal field theory data for transition-metal ions.

No. of d-electrons	Ion	Free ion	Octahedral	Tetrahedral	D_q oct.	D_q (cm^{-1}) tetr.
			Ground state			
3	Cr^{3+}	^4F	$^4A_{2g}$	$^4T_{1g}$	1 760	780
4	Cr^{2+}	^5D	^5E_g	$^5T_{2g}$	1 400	620
5	Fe^{3+}	^6S	$^6A_{1g}$	$^6A_{1g}$	1 400	620
6	Fe^{2+}	^5D	$^5T_{2g}$	^5E_g	1 000	440

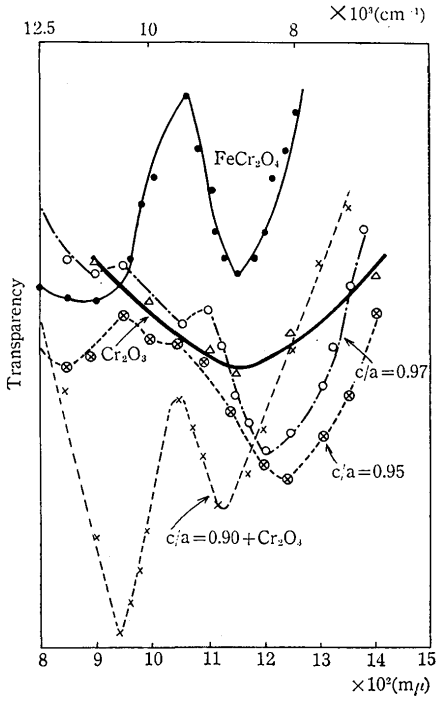

Fig. 24. Near-infrared absorption results.

the energy level of chromium atom induced by the interaction of electron between chromium and the other atoms composing the crystal.

An enlarged portion of Fe-Cr-O diagram at 1600° C is given in **Fig. 25.** It is seen that the region of tetragonal chromite does not extend to the composition of Cr_3O_4.

To confirm an applicability of physical measurements to clarify the formation mechanism of tetragonal chromite, a perfect single crystal should be used.

The results are as follows:

(1) The tetragonal iron chromite contains more chromium than the stoichiometric $FeCr_2O_4$ composition and the axial ratio becomes smaller with increase of chromium and decrease of oxygen partial pressure.

(2) Cubic and tetragonal chromites have defect structures and the role of iron to give the tetragonal structure was clarified.

(3) Cr^{2+} valence state is probably possible but the existence of Cr_3O_4 or CrO is not obvious, although the previous studies suggested it.

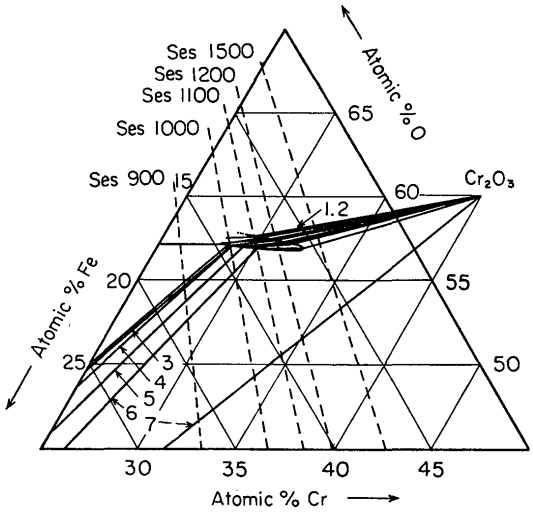

Fig. 25. An enlarged portion of Fe-Cr-O diagram at 1600°C.

4. Complex Deoxidation

Hilty and Craft[148] have recognized that complex deoxidant of aluminium + silicon plays more effective action than aluminium when deoxidation of 0.46 % manganese containing steel was carried on. This superior action is shown in **Fig. 26.**

Furthermore, the deoxidation effect of complex deoxidant of aluminium + manganese + silicon is the most remarkable. In **Fig. 27,** this excellent action is shown too.

Koch, Wentrup and Reif have studied about the

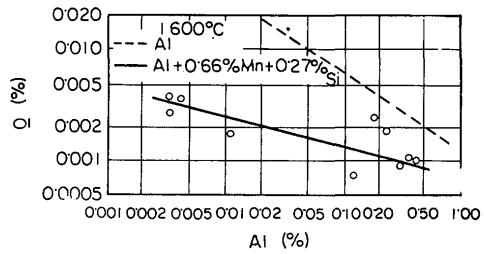

Fig. 26. Effect of complex deoxidant of Al +Mn +Si.[148]

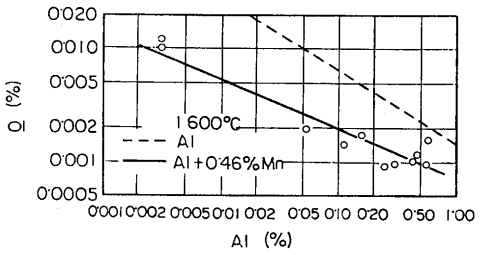

Fig. 27. Effect of complex deoxidant of Al+Mn.[148]

complex deoxidation products in detail by comparing the phase diagram of aluminium + manganese + silicon.[149] According to their results, silicate · glass containing much aluminium is formed when the deoxidizer of $Mn/Si<2$ was used. On the other hand, solid crystals containing much Al_2O_3 is formed when the deoxidant of $Mn/Si>2$ was used.

In regards to the complex deoxidation, it is important to consider the problem of the flotation of inclusions in the molten steels to get good deoxidation action. Mukai, Sakao and Sano have given consideration from the standpoints of surface tension measurement[150), 151)]

For a long time, the problem of the flotation of inclusions in the molten steels have been discussed. Recently, the effect of calcium addition to complex deoxidant have been investigated. Asano and Nakano[152)] have reported that the shape of the deoxidation products become spherical when complex deoxidant of aluminium + calcium + silicon + manganese was used, but the shape change to crowdy when aluminium + magnesium + silicon as well as aluminium was used. The latter is more effective to decrease oxygen content in steel than the former, they say that these difference is reduced to the flotation velocity of the inclusions formed.

Shiraiwa and Fujino have investigated the complex deoxidation, and they have concluded that the following effects were determined from the results by electron probe microanalyzer[153)].

bonding strength with oxygen: Al > Ca > Si > Mn,
with sulphur: Ca > Mn > Al
with calcium: O > S
with manganese: S > O

Although the appearence of electron probe microanalyzer has been considered to play effective roll to analyze complex deoxidation, there remains many unresolved problems now.

Subsequently, the results obtained concerning chromium steels are briefly summarized.

1) Silicon addition

Usually, cubic chromite ($FeCr_2O_4$) is formed in steel containing chromium. When 0.3 % silicon was added, Cr_2O_3 and α-quartz appeared besides predominant cubic chromite.

As deoxidation reaction,

$$2FeCr_2O_4 + Si = 2Cr_2O_3 + 2SiO_2 + 2Fe \quad (3)$$

must be given.

While, although tetragonal chromite ($c/a=0.89$) appears at the case of 17 % chromium containing steel lesser amounts of tetragonal chromite, Cr_2O_3, α-quartz and α-tridymite appeared. Transformation behaviour of SiO_2 formed in steels is the most interesting problem.

The fact that chromium silicate which is usually found in slag of Fe-Cr-Si-O system did not appear in steels suggest that the equilibrating oxygen partial pressure is higher for the appearence.

2) Manganese addition

When added 1.5 % manganese to 1 % chromium containing steel, $MnFe_2O_4$ which seems uncertainly and Mn_3O_4 appeared besides cubic chromite. It will be anticipated that the equilibrating oxygen partial pressure in the case is considerably higher.

While, $MnCr_2O_4$ which appear usually has been only detected at the case of 17 % chromium containing steel.

Application of potentiostatic decomposition of carbide to make identification of oxide inclusion formed in steel easily.

First, usual extraction method using 5 % sodium citrate and 1.2 % potassium bromide aqueous solution or 10 % hydrochloric acid - ethyl alcohol solution as electrolyte was used for 18-8 Cr-Ni stainless steel. In **Fig. 28,** X-ray diffraction patterns of the residues extracted from SUS 38 stainless steel are compared with the one for synthetic chromium carbide ($Cr_{23}C_6$). As a

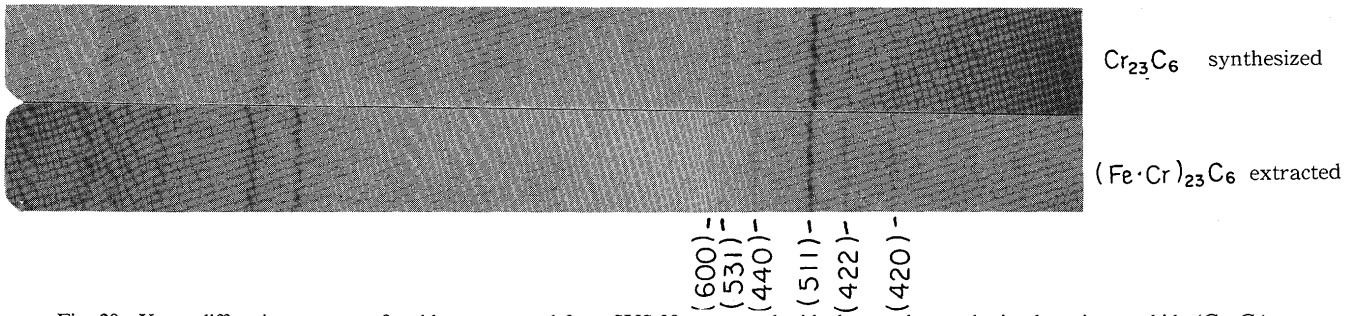

Fig. 28. X-ray diffraction pattern of residues extracted from SUS 38 compared with the one by synthetic chrominm carbide ($Cr_{23}C_6$) (Cr K_α).

result, we can recogneize that informations about oxide or sulphide inclusions formed are not obtained by the disturbance of carbide extracted in the case of steels for practical use.

So, it was necessitated to separate carbide from oxide or sulphide inclusions by the application of some means.

We have considered if decomposition of carbide formed in steels in the electrolytic process are possible with the suitable choice of electrolyte.

Previously, Koch and Sundermann reported[30] the success of measurement of polarizing characteristic of specimen made from some binder and cementite extracted from steel. However, polarizing characteristics of specimens depend upon their surface conditions and sample history therefore, we should consider if manufacturing method like this is appropriate for electrochemical measurement. For this raeson, it is necessary to make specimens sintered well with minimized binder or without it.

We synthesized chromium carbides, Cr_3C_2, Cr_7C_3 and $Cr_{23}C_6$ from graphite and chromium powder at the temperature of 1450–1850°C in the stream of refined hydrogen.

We compared the polarizing characteristics of various sorts of chromium steels, 18-8 Cr-Ni stainless steel and the above synthesized chromium carbide.

The polarizing results in 3 % potassium bromide aqueous solution are shown in **Fig. 29.** From this, we can understand that chromium carbide is safely extracted by weak acidic electrolyte.

In **Fig. 30,** the results in 3 % ammonium fluoride aqueous solution are shown. Similarly, the stability of chromium carbide is established by this method.

However, this situation changes when 10 % hydrophosphoric aqueous solution is used. The results are shown in **Fig. 31.**

Likewise, X-ray diffraction patterns of inclusions extracted from niobium containing stainless steel in market are compared with the compound synthesized

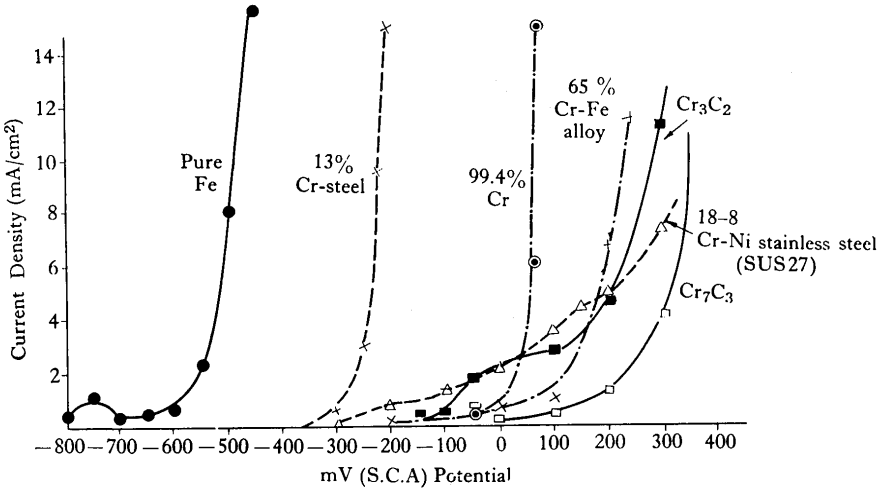

Fig. 29. Polarizing characteristics of chromium carbide and iron-chromium alloys when 3 % potassium bromide aqueous solution is used.

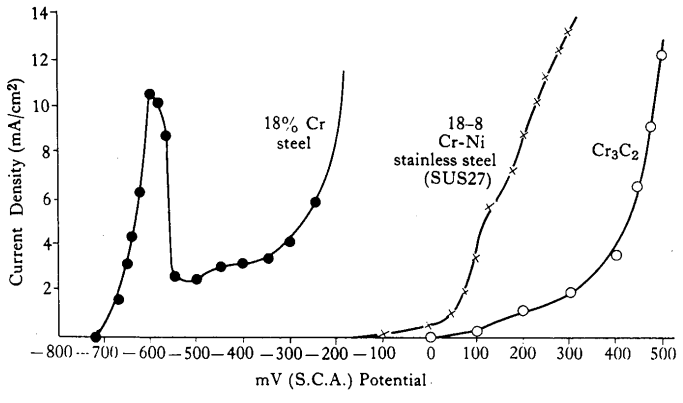

Fig. 30. Polarizing characteristics of chromium carbide, 18 % chromium steel and 18-8 Cr-Ni stainless steel when 3 % ammonium fluoride aqueous solution is used.

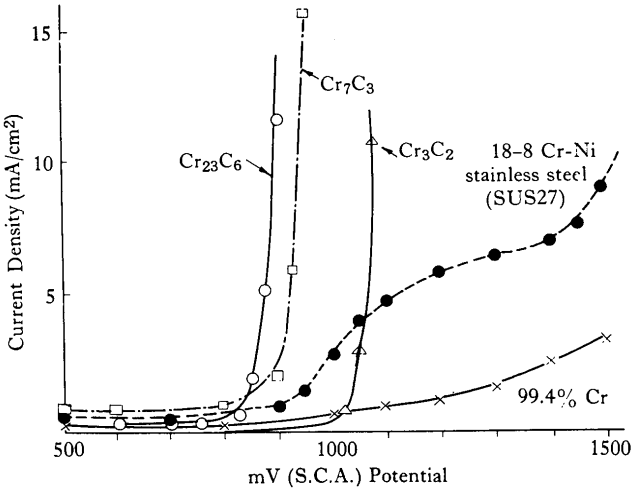

Fig. 31. Polarizing characteristics of chromium carbide, pure chromium and 18-8 Cr-Ni stainless steel when 10 % hydrophosphoric acid aqueous solution is used.

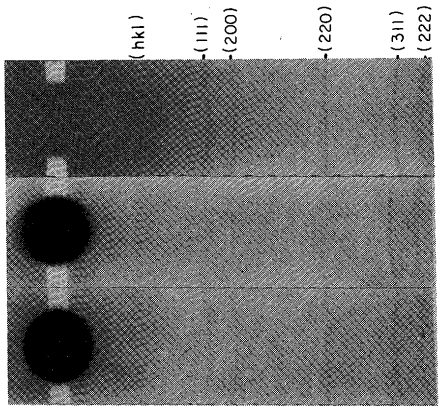

Fig. 32. Inclusions extracted from SUS 43.

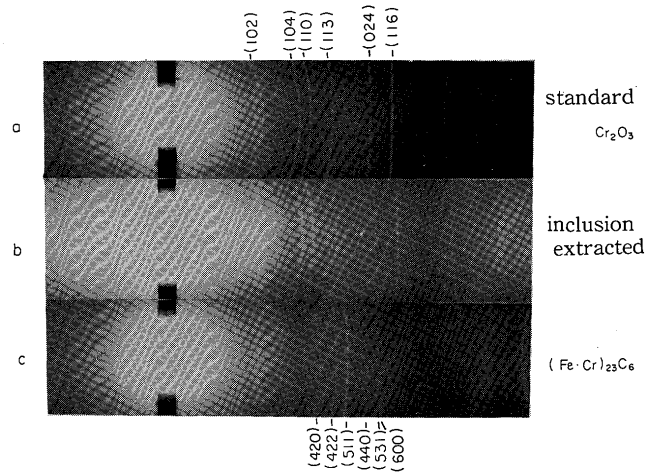

XFig. 33. X-ray diffraction pattern by resudies, extracted from SUS 27 with the use of 10 % hydrophosphoric acid aqueous solution, is compared with the one form chromic oxide and chromium carbide extracted (Cr K_α).

in **Fig. 32.**

Summarizing the results above described, we have performed electrolytic extraction with 10 % hydrophosphoric acid aqueous solution to SUS 27 stainless steel under the potentiostatic condition of 1.3 V. This result is shown in **Fig. 33.**

Acknowledgement

Author thank to Professor emeritus of Osaka University, Dr. Akira Adachi for his kindly support for my works and thank to ardent assistances from Messrs. S. Shizima, Y. Ueda, M. Ueda, M. Kitamura, H. Kanayama, H. Kumon, K. Michishita, M. Takano, H. Yoshida, H. Matsumoto, I. Yoshinaka, T. Kawahara and S. Oojiri.

References

109) Von G. Brauer and R. Esselborn: Z. anorg. allge. Chem., 308, (1961), p. 52.
110) R. P. Flliott: Trans. ASM, 52 (1960), p. 990.
111) R. W. Guard, J. W. Savage and D. G. Swarthout: Trans. AIME, 239 (1967), p. 643.
112) G. Brauer u R. Lesser: Z. Metallk., 50 (1959), p. 8.
113) G. Brauer u R. Lesser: Z. Metallk., 50 (1959), p. 487.
114) E. K. Storms and N. H. Krikorian: J. Phy. Chem., 64 (1960), p. 1471.
115) T. Mori, S. Tokizane, K. Yamaguchi, E. Sunami and Y. Nakajima: Tetsu to Hagane, 54 (1968), p. 763.
116) G. Brauer: J. Less-Common Metals, 2 (1960), p. 131.
117) A. C. Turnock: J. Amer. Ceram. Soc., 49 (1966), p. 177.
118) E. F. Bertaut, L. Corliss, F. Forrat, R. Aleonard · and R. Pauthenet: J. Phy. Chem. Solids., 21 (1961), p. 234.
119) A. C. Turnock: J. Amer. Ceram. Soc., 48 (1965), p. 259.
120) A. L. Bowman, T. C. Wallace, J. L. Yarnell and R. G. Wenzel: Acta. Cryst., 21 (1966), p. 843.
121) W. Jäger, A. Rahmel and R. Korn: Arch. Eisenhütenw., 34 (1963), p. 279, 291.
122) G. Brauer: Z. anorg. Chem., 248 (1941), p. 1.
123) C. E. Sims and CH. W. Briggs: J. Metals, 11 (1959), p. 815.
124) P. Duwez, F. Odell and F. H. Brown Jr.: J. Amer. Ceram. Soc., 35 (1952), p. 107.
125) P. Duwez, F. H. Brown Jr. and F. Odell: J. Electrochem. Soc., 98 (1951), p. 356.
126) W. C. Wyder and M. Hogh: Trans. AIME, 224 (1962), p. 373.
127) R. Ruh: J. Amer. Ceram. Soc., 46 (1963), p. 301.
128) B. C. Wever, H. J. Garrett, F. A. Maner and M. A. Schwarz: ibid., 39 (1956), p. 197.
129) G. M. Wolton: ibid., 46 (1963), p. 418.
130) D. C. Hilty, W. J. Forgeng · and R. L. Folkman: J. Metals, 7 (1955), p. 253.
131) M. Hansen: Constitution of Binary Alloys, 2nd ed., (1958), McGraw-Hill, New York.
132) F. Körber and W. Oelsen: Mitt-Kais-Wilh-Inst. Eisenforsch., 17 (1935), p. 231.
133) C. E. Sims, H. A. Saller and F. W. Boulger: Trans. AIME, 185 (1949), p. 814.
134) B. W. Linchevskij and A. M. Samarin: Izv. Akad. Nauk SSSR Otd. Tek. Nauk, (1953), p. 691.
135) R. E. Johnson and A. Muan: J. Amer. Ceram. Soc., 51 (1968), p. 430.
136) J. S. Griffith: Theory of Transition-Metal Ions, 2nd ed., (1964), Cambridge, London.
137) R. A. Jahn and E. Teller: Proc. Roy. Soc., A161 (1937), p. 220.
138) J. D. Dunitz and L. E. Orgel: J. Phys. Chem. Solids, 3 (1957), p. 20.
139) H. Oonishi and T. Teranishi: J. Phys. Soc. Japan, 16 (1961), p.35.
141) S. Chikazumi ed: Progress in Magnetic Physics, AGNE, Tokyo, (1964). (in Japanese)
141) G. K. Weltheim: Application of the Mössbauer Effect in Chemistry and Solid State Physics, (1966), International Atomic Energy Agency, Vienna.
142) S. Tanaka and G. Okuno: Japan J. Phys., 9 (1934), p. 75.
143) S. Tanaka and G. Okuno: Proc. Phys., Math. Soc. Japan, 17 (1935), p. 540.
149) A. Meisel and W. Nefedow: Z. anorg. allg. Chem., 339 (1965), p. 1.
145) A. Z. Men'shikov and S. A. Nemonov: Phys. of Metals and Metallog., 14 (1962), p. 23.
146) A. Meisel and To Ba Trong: J. Prak. Chem., 29 (1965), p. 192.

147) T. M. Dunn, D. S. McClure and R. G. Pearson: Some Aspects of Crystal Field Theory, Harper and Row and John Weatherhill, Inc., Tokyo (1965).

148) D. C. Hilty adn W. Grafts: J. Metals, 188 (1950), p. 414, 425.

149) W. Koch, H. Wentrup and O. Reif: Arch. Eisenhüttenw., 22 (1951), p. 15.

150) K. Mukai, H. Sakao and K. Sano: J. Japan Inst. Metals, 31 (1967), p. 928. (in Japanese)

151) K. Mukai, H. Sano and K. Sano: ibid, 32 (1968), p. 1155 (in Japanese)

152) K. Asano and T. Nakano: Tetsu to Hagane, 57 (1971), p. 1943. (in Japanese)

153) T. Shiraiwa and M. Fujino: ibid, 57 (1971), p. 1990. (in Japanese)

154) A. Adachi and N. Iwamoto: Trans. ISIJ, 6 (1966), p. 417.

155) N. Iwamoto and A. Adachi: ibid, 9 (1969), p. 59.

156) A. Adachi and N. Iwamoto: The 2nd Japan-USSR Joint Symp. on Physical Chemistry of Met. Proc. (1969).

157) N. Iwamoto, M. Takano and A. Adachi: Tetsu, to Hagane, 56 (1970), p. 716. (in Japanese)

158) N. Iwamoto, M. Takano, H. Kanayama and A. Adachi: ibid, 56 (1970), p. 727. (in Japanese)